CHAPTER 24

VARIATION OF POTENTIAL AND KINETIC WAVE ENERGY IN THE SURF ZONE

Koichiro IWATA* and Takashi TOMITA**

ABSTRACT

This paper is to investigate experimentally variation of the potential and kinetic wave energy in the surf zone. First, a cantilever-type velocimeter is newly devised to measure water particle velocities in an air-entrained water body above as well as below the wave trough. Laboratory experiments are carried out, and it is revealed that the kinetic wave energy is larger than the potential one and that some of the potential wave energy can be transferred to the kinetic one at the early stage of wave breaking.

1. INTRODUCTION

Prediction of variation of the wave energy such as potential, kinetic and total wave energy and elucidation of wave dissipation mechanism in the surf zone is one of very important problems for coastal hydraulics as well as coastal engineering. A lot of knowledge about wave breaking and wave deformation after breaking have been accumulated,but it is still unknown how the potential and kinetic wave energy change and how we estimate them well in the surf zone. In particular, an accurate evaluation of the kinetic wave energy is very useful for prediction of the nearshore current system.

---

* M.ASCE, D.Eng., Professor, Dept. of Civil Eng., Nagoya Univ.,Nagoya 464-01, Japan

** D.Eng., Research Associate, ditto

With this background, this paper discusses experimentally the variation of potential and kinetic wave energy in the surf zone. First of all, a cantilever-type velocimeter is newly devised in order to measure the kinetic wave energy as well as particle velocities in the air-entrained wave body above and below the wave trough. Secondly, laboratory experiments are conducted on the uniform slopes of 1/10 and 1/30, using an indoor wave tank which can generate regular and irregular waves. Based on the laboratory experiments, characteristics of variation of the potential and kinetic wave energy, the wave energy dissipation and the propagation velocity of the total wave energy in the surf zone are discussed in relation to breaker types and breaker-caused turbulence.

2. CANTILEVER-TYPE VELOCIMETER

A cantilever-type velocimeter based on the " dynamic pressure principle" is newly devised in order to measure accurately the water particle velocity, especially above the wave trough in the surf zone, since we have no reliable velocimeter which enables us to measure wave kinematics above wave trough including air-bubble and turbulence.

The cantilever-type velocimeter is comprized of two cantilevers, as shown schematically in Fig.1,one of which only responds to a vertical component of the dynamic force and another responds only to a horizontal component of the dynamic force. Each cantilever is constructed with a small-sized sensing rod and a plastic plate which is rigidly fixed to a supporting rod. Two semi-conductor strain gauges are pasted on the plastic plate to convert the wave force acting normally to the cantilever into an electrical signal. The plastic plate and end part of the sensing rod is protectively shielded so as not to be affected by direct attack of waves. The diameter of the sensing rod was carefully designed to 0.9mm in order to respond to the fluid drag force and to be almost insensitive to the fulid acceleration force.

Figure 2 shows that the wave force acting on the sensing element is proportional to square of the velocity. Therefore, the water particle velocities, u and w are calculated with

$$\begin{aligned} u|u| &= \left(\frac{Xo}{Kx}\right)\left|\left(\frac{Xo}{Kx}\right)\right| \Big/ \sqrt{\left(\frac{Xo}{Kx}\right)^2 + \left(\frac{Zo}{Kz}\right)^2} \\ w|w| &= \left(\frac{Zo}{Kz}\right)\left|\left(\frac{Zo}{Kz}\right)\right| \Big/ \sqrt{\left(\frac{Xo}{Kx}\right)^2 + \left(\frac{Zo}{Kz}\right)^2} \end{aligned} \qquad (1)$$

where, u and w are the horizontal and vertical velocities of water particle, respectively, Xo and Zo are the output voltages of horizontally and vertically sensing cantilevers, respectively, and Kx and Kz are the correction factors to Xo and Zo which are determined by calibration tests, respectively. High accuracy of this cantilever-type velocimeter has been confirmed by comparing with data obtained with electro-magnetic-type velocimeter. as shown in Fig.3 (Iwata et al., 1983 and Koyama and Iwata,1986).

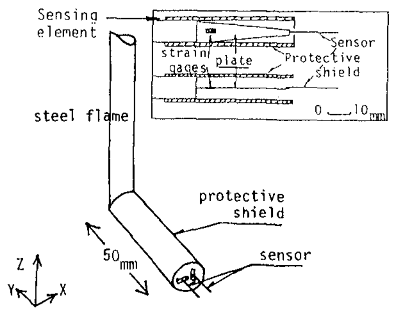

Fig.1 Schematic illustration of cantilever-type velocimeter

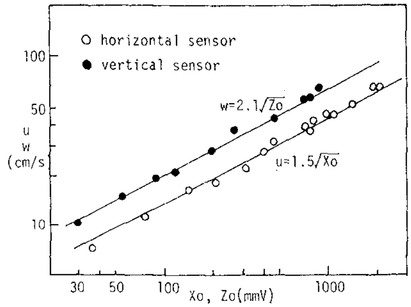

Fig.2 Calibration test curves

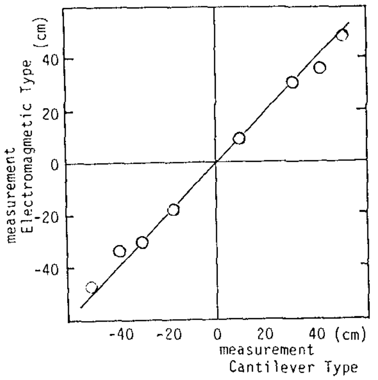

(a) amplitude of velocity

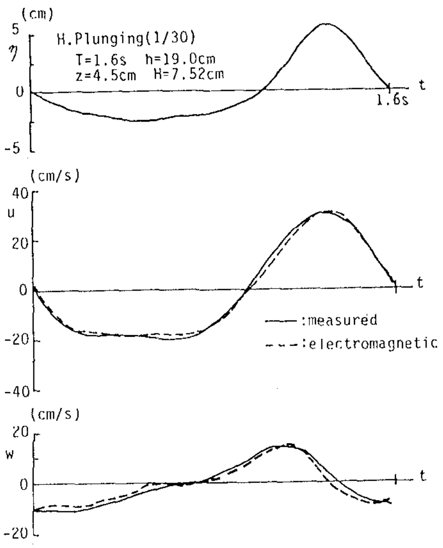

(b) time histories of water particle velocities,u and w, and water surface profile, η

Fig.3 Comparison of velocities of water particle measured with cantilever-type and electromagnetic-type velocimeters

3. LABORATORY EXPERIMENT

Laboratory experiments were carried out using an indoor wave tank at Nagoya University, the dimension of which is 25m in length, 0.7m in width and 0.95m in height. At one end of the wave tank we installed a flap-type wave generator controlled by an oil-pressure servo system. The water was perfectly shut out from the area behind the wave board; therefore, the input electrical signal can be converted smoothly to wave board motion. At the other end of the wave tank was constructed a wave-absorbing beach to keep wave reflection to a minimum. The uniform slopes of 1/10 and 1/30 were adopted and three kinds of breakers such as spilling, plunging and heavy plunging were produced on each slope (see Table 1).

Water surface profiles and particle velocities were, respectively, measured with capacitance-type wave gauges and cantilever-type velocimeters. The measuring locations of water particle velocities were more than 126, as listed in Table 1. The measuring region was from near bottom up to near free surface in vertical direction and from before the wave breaking point to near shoreline in horizontal direction. In the experiments, the same wave was generated repeatedly in order to measure particle velocities at so many locations. One example of the measuring locations is shown in Fig.4. For each experimental run, using a 16mm high speed cine camera (50 frames/s), breaking region was filmed through a grid on glass wall of the channel. Analyzing the films, the breaking point, domain of horizontal roller, and region of air-entrainment were determined. Time profiles of water surface and particle velocities were all recorded on a magnetic tape over 2 minutes.

Table 1 Experimental conditions

CASE	BREAKER	SLOPE	T(s)	Ho(cm)	Ho/Lo	Hb(cm)	h_b(cm)	M
1-1	Spilling	1/10	0.95	17.0	0.120	14.0	26.0	126
1-2	Plunging	1/10	1.35	16.9	0.060	14.4	18.8	130
1-3	H.Plunging	1/10	1.35	15.7	0.055	13.4	14.8	146
2-1	Spilling	1/30	1.00	10.5	0.067	10.1	16.0	186
2-2	Plunging	1/30	1.45	7.0	0.021	9.1	13.3	169
2-3	H.Plunging	1/30	1.60	7.1	0.018	9.0	13.7	188

T: wave period, Ho:deep water wave height, Ho/Lo:wave steepness in deep water, Hb:breaking wave height, h_b:breaking water depth
M: measuring locations of water particle velocity

4. DATA PROCESSING AND ANALYSIS

Time profiles of the water surface profile and particle velocities were divided into 20 discrete values for one wave

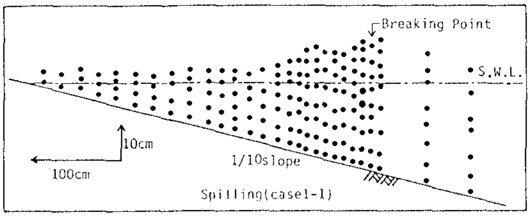

Fig.4 Measuring locations of water particle velocity for case 1-1

cycle to evaluate the potential and kinetic wave energy.

The mean water level $\bar{\eta}$ is estimated with

$$\bar{\eta} = \frac{1}{T}\int_0^T \eta dt \qquad (2)$$

in which, T is the wave period and η is the water surface profile.

The potential wave energy per unit time averaged over one wave period, Ep and kinetic wave energy per unit time averaged over one wave period, Ek are, respectively, defined with

$$Ep = \frac{\rho g}{2T}\int_0^T \eta^2 dt \qquad (3) \qquad Ek = \frac{\rho}{2T}\int_0^{h+\eta} ds\int_0^T (u^2 + w^2)dt \qquad (4)$$

in which, ρ is the density of water, g is the gravitational acceleration, h is the still water depth, s is the vertical distance taken upward positive with its origin being on the bottom, u and w are the horizontal and the vertical of water particle, respectively. The total wave energy per unit time averaged over one wave period, E_T is given by

$$E_T = Ek + Ep \qquad (5)$$

The energy flux, F and the energy dissipation rate, Φ are evaluated with the following equations;

$$\frac{\partial}{\partial x}(F) = - \Phi \qquad (6)$$

$$F = \frac{1}{T}\int_0^T dt\int_0^{h+\eta} u(\frac{\rho}{2}(u^2 - w^2) + \rho g\eta)ds \qquad (7)$$

where, x is the horizontal distance, and Eq.(7) is derived for the second-order approximation of wave pressure, P. The calculations of Ep, Ek and F were performed by applying the trapezoidal formula to Eqs.(3),(4) and (7), respectively, using measured vaues of η, u and w.

Analysing 16mm motion films by means of a film motion analyzer, the breaking point, air-entained region, plunging point, domain of horizontal roller, splash zone were determined. The breaking point is defined just as the inception of curling of wave crest. Therefore, the breaking point corresponds to the maximum wave height.

3. EXPERIMENTAL RESULTS AND DISCUSSION

3.1 Water particle velocity

Figures 5 and 6 show two examples of water particle velocities before and after wave breaking. It is seen that measured velocities are well predicted with Dean's stream

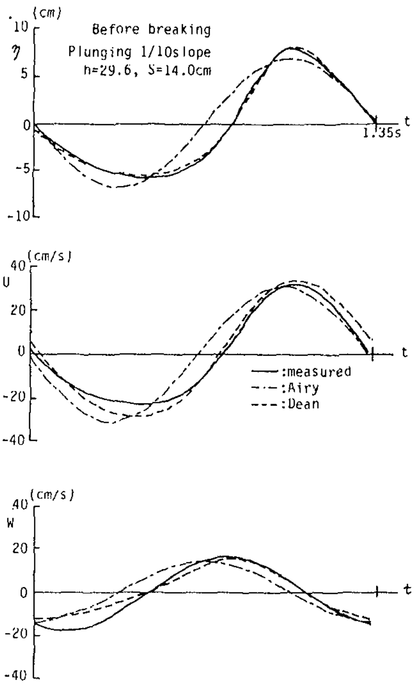

Fig.5 Time histories of water particle velocities (before breaking)

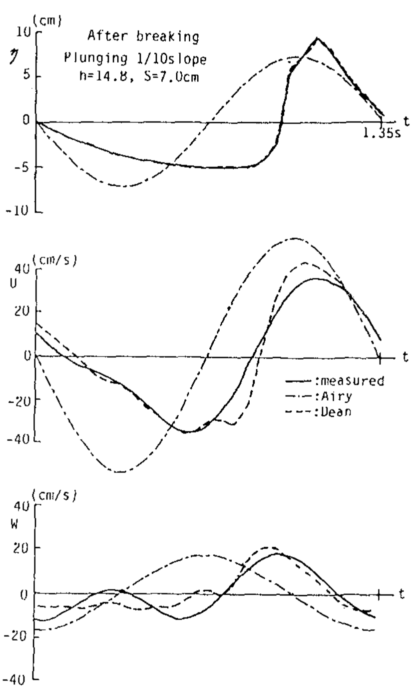

Fig 6 Time histories of water particle velocities (after breaking)

function method (Dean,1965). However, Airy's linear wave theory cannot well evaluate the water particle velocities. Figure 7 shows the time profile of water particle velocities measured at 5cm above the still water level. The particle velocity profiles are quite similar to those of the solitary wave above wave trough (Lee et al.,1982). Figure 8 shows examples of the vertical distribution of the horizontal steady-velocity component, $\bar{u}$ at three different locations such as before breaking, breaking point and after breaking. The steady-velocity component $\bar{u}$ is the velocity which is averaged over one wave period both above and below the wave trough. From the figures, it is seen that the onshore mass transport takes place above the wave trough and offshore mass transport occurs below the wave trough and that conservation of mean mass flux is established. The magnitude of the steady-velocity component (mass transport velocity) corresponds well to foregoing researches (Nadaoka et al.,1982). Thus, as described above, the cantilever type velocimeter devised in this study can safely be said to be highly reliable to measure water particle velocities.

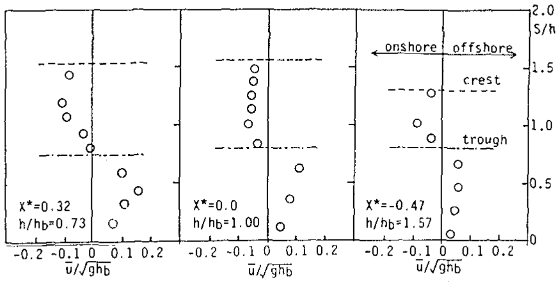

Fig. 8 Some examples of vertical distribution of horizontal steady-velocity component, $\bar{u}/\sqrt{gh_b}$ (h/h_b=1.57;before breaking, h/h_b=1;breaking point, h/h_b=0.73;after breaking)

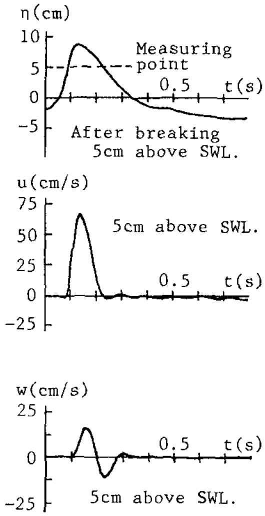

Fig.7 Time histories of water particle velocities measured at 5cm above the still water level

3.2 Variation of potential and kinetic wave energy

Figures 9 shows the variation of the wave height after breaking. Both figures show that the wave height decreases almost monotonously toward the shoreline, as have been pointed out by foregoing researches(Horikawa and Kuo,1966; Sawaragi and Iwata,1974).

Figures 10,11 and 12 show the variation of the potential and kinetic wave energy after breaking in cases of the spilling, plunging and heavy plunging breaker, respectively. In the figures, $X^*=(x-x_b)/\sqrt{g(h+\bar{\eta})}T$, x_b is the breaking location of x (X^*=0;breaking point), Etb is the total wave energy at breaking point, Xa is the location of deepest air entrainment, Xo is the location of air bubble's disappearance below wave trough, Xp is the plunging point, Xs is the location of horizontal roller's disappearance and Xv is the location at which air bubble covers the front face from crest

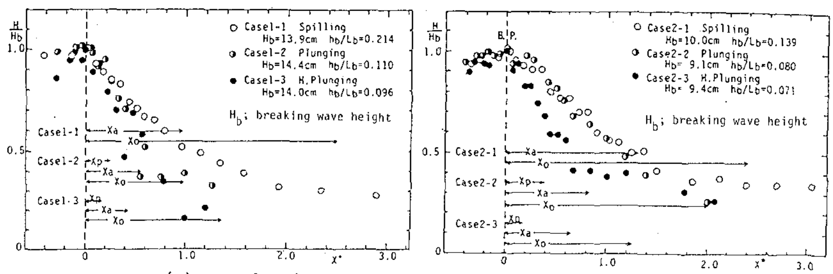

(a) $\tan\theta$ =1/10 (b) $\tan\theta$ =1/30

Fig.9 Variation of the wave height after breaking to trough. The symbols, ○ , ■ and △ are experimental values of E_T/E_{Tb}, Ek/E_{Tb} and Ep/E_{Tb}, respectively.

(a) Spilling breaker:

The potential wave energy Ep decreases monotonously from X*=0 to X=Xa at which the entrained air depth is maximal for both slopes of 1/10 and 1/30. The potential wave energy Ep at X*=Xa is almost 0.3Epb (Epb;Ep at X*=0). This indicates that almost 70% of the potential wave energy at breaking point is dissipated from X*=0 to X*=Xa. On the other hand, decay of Ep in the range of X*>Xo is seen to be very small.

The kinetic wave energy Ek is clearly seen to be larger than tha potential one, and Ek increases at an early stage of wave breaking and then decreases toward the shoreline. This is quite different from the change of Ep with X*. The kinetic wave energy Ek around X*=0.2 becomes larger than that at X*=0. This fact would indicate that some of the potential wave energy is transferred to the kinetic one, since the potential wave energy continuously decays around X*=0.2. The attenuation of Ek in the range of X*>Xo is very small and Ek is almost equal to Ep. The magnitude of difference between Ek and Ep increases with X* in the range of X*<Xa and Ek/Ep becomes maximal around X*=Xa; Ek/Ep≅2.7 for case 1-1 and Ek/Ep≅2.4 for case 2-1. The value of Ek/Ep at breaking point is 1.15 for case 1-1 and 1.08 for case 2-1. These values are smaller than those measured on gentler slope of 1/150 by Tsuchiya and Tsutsui (1982).

The total wave energy E_T decays monotonously from X*=0 to X*=Xo, although Ek increases around X*=0.2. Figure 10 shows that 70% ∿ 80% of E_{Tb} (total wave energy at breaking point) are dissipated between X*=0 and Xo.

(b) Plunging breaker:

Rapid decay of the potential wave energy Ep takes place from X*=Xp to X*=Xa, and Ep at X*=Xa attenuates to 0.6Epb for case 1-2 and 0.3Epb for case 2-2. The magnitude of attenuation of Ep on S=1/10 is larger than that on S=1/30, where S is the bottom slope.

The kinetic wave energy Ek after breaking is seen to be smaller than that at breaking point Ekb. In case of 2-2(S=1/30), Ek attenuates monotonously and the magnitude of decay of Ek between X*=0 and Xa is much larger than that in the range of X*>Xa. On the other hand, in case of 1-2 (S=1/10), Ek once increases around X*≅Xa. The reason of this is thought to be that the energy of splash and horizontal roller is transferred to the kinetic energy. Then, the total wave energy E_T becomes also larger around X=Xa in case of run 1-2.

(c) Heavy plunging breaker:

The potential wave energy Ep decreases rapidly after breaking and Ep around X*=Xs becomes 0.25Epb. The potential wave energy once increases around X*=Xa. This is thought to be caused by the combination of splash with main

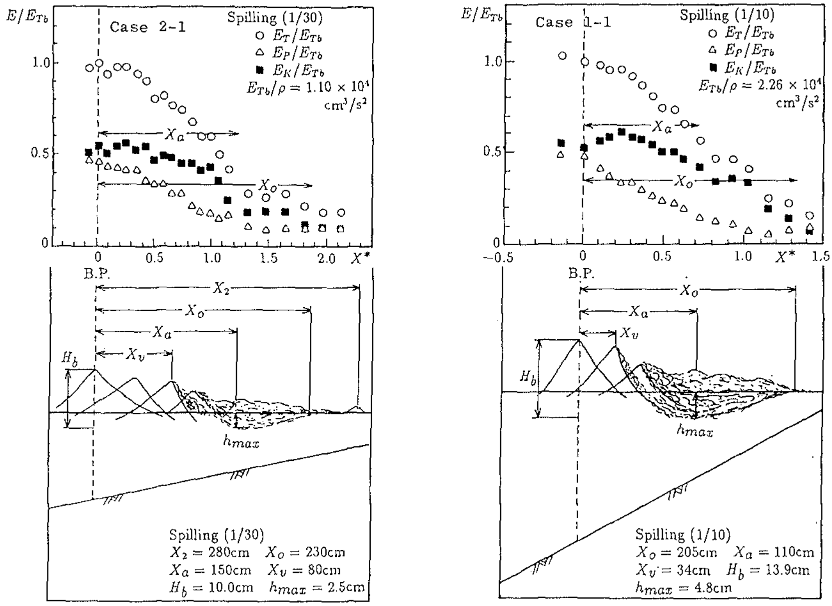

Fig.10 Variation of potential and kinetic wave energy after breaking (Spilling breaker)

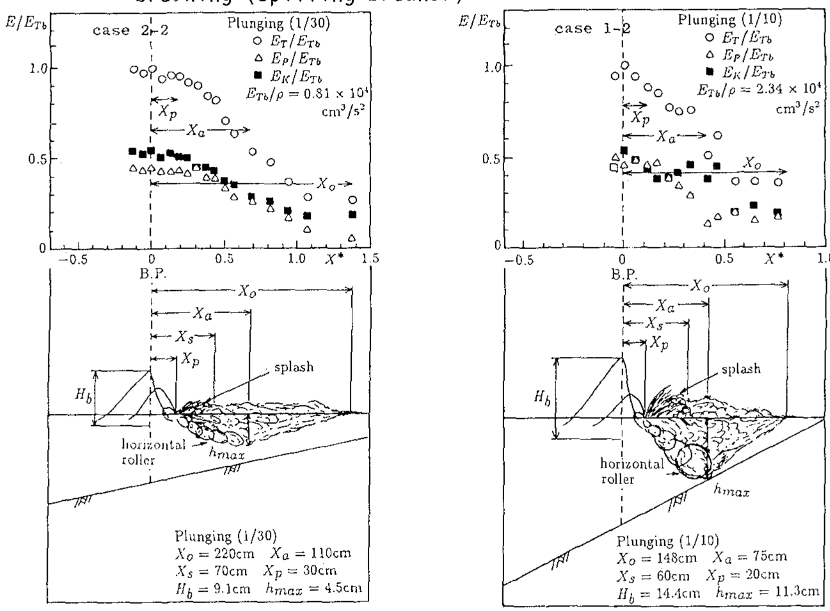

Fig.11 Variation of potential and kinetic wave energy after breaking (Plunging breaker)

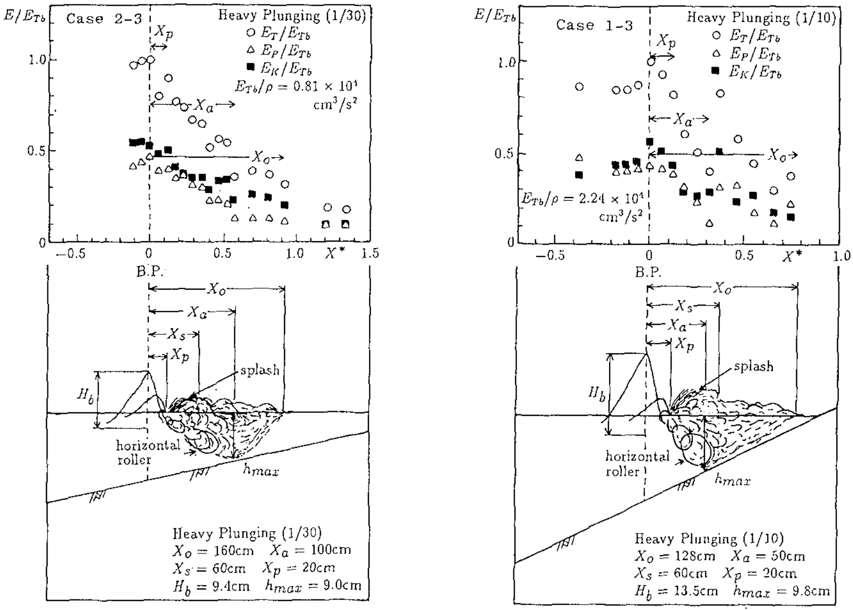

Fig.12 Variation of Potential and kinetic wave energy after breaking (Heavy plunging breaker)

wave body.

The kinetic wave energy Ek decays rapidly within the short distance between X*=0 and X*=Xp, and 50% and 25% of Ekp are dissipated, respectively, in the cases of 1-3 and 2-3 in this range. The kinetic wave energy Ek once increases between X*=Xa and X*=Xs where the splash and horizontal roller's energy seem to be combined with the main wave body. The attenuation of Ek in the range of X*>Xo is very small, like the spilling and plunging breakers.

The total wave energy E_T decreases rapidly after breaking and once increases between X*=Xa and X*=Xs, like the plunging breaker. Attenuation of E_T from X*=Xa is small, like the spilling and plunging breakers. The kinetic wave energy Ek is generally larger than the potential wave energy Ep and the ratio of Ek/Ep becomes larger with X* and takes a maximum value between X*=Xs and X*=Xa and then decreases to 1, like other types of breakers. The maximum value of Ek/Ep in case of 1-3 is 1.62.

As stated above, regardless of breaker types, most of the potential and kinetic wave energy are dissipated from breaking point (X*=0) to X*=Xo, especially rapid energy dissipation takes place between X*=0 and X*=Xa at which the depth of entrained air bubble becomes maximum. Thus, it seen that qunatity of air bubble is an index of wave energy dissipation.

3.3 Variation of energy flux

Figures 13 and 14 show changes of the nondimensional energy flux F/Fb with X*, where Fb is the energy flux at breaking point. The magnitude of changes of F/Fb with X* depends on breaker types and botton slopes. The figures show that F/Fb attenuates in the order of spilling, plunging and heavy plunging breakers and that the decay of F/Fb in the range of $0 \leq X^* \leq Xa$ is much larger than that in the range of $X^* \geq Xa$. The splash and horizontal roller are only formed in cases of plunging and heavy plunging breakers and their scale of the heavy plunging breakers are larger than those of the plunging breakers. This causes the most rapid decay of F/Fb of the heavy plunging breaker among the three breakers. Figure 15 shows the relationship between F/ρ and d $(=h+\bar{\eta})$, in which the solid and dotted lines indicate, respectively, Eq.(8) and Eq.(9). γ in Eq.(8) and γ and β in Eq.(9) were determined by a least square method, and they

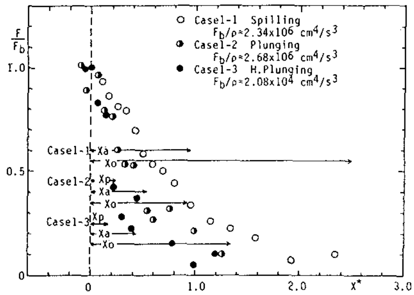

Fig.13 Variation of F/Fb with X* (S=1/10)

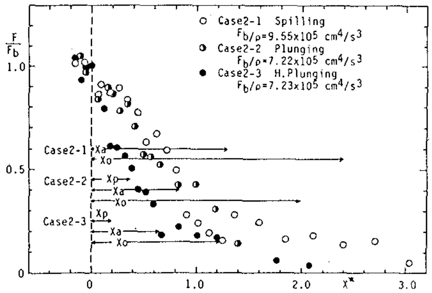

Fig.14 Variation of F/Fb with X* (S=1/30)

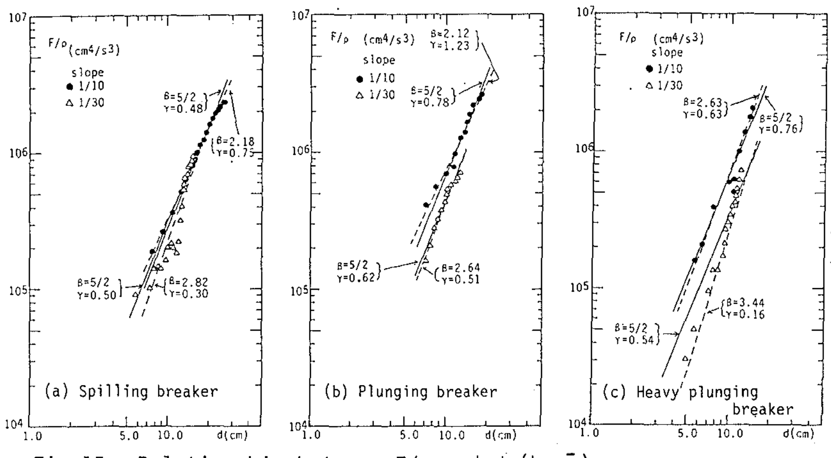

Fig.15 Relationship between E/ρ and d $(h+\bar{\eta})$

are given in Table 2.

$$\frac{F}{\rho}=\frac{1}{8}g^{\frac{3}{2}}\left(\frac{H}{d}\right)^{\gamma}(d)^{\frac{5}{2}} \qquad (9)$$

$$\frac{F}{\rho}=\frac{1}{8}g^{\frac{3}{2}}\left(\frac{H}{d}\right)^{\gamma}(d)^{\beta} \qquad (10)$$

Table 2 Values of β and γ

	β	γ	β	γ
Spilling(1/10)	5/2	0.48	2.18	0.75
Plunging(1/10)	5/2	0.78	2.12	1.23
H.Plunging(1/10)	5/2	0.76	2.63	0.63
Spilling(1/30)	5/2	0.50	2.82	0.30
Plunging(1/30)	5/2	0.62	2.64	0.51
H.Plunging(1/30)	5/2	0.54	3.44	0.16

$\gamma=2$ and $\beta=5/2$ are derived for the linear long wave theory (Ishii,1990). Table 2 shows that γ is much smaller than 2, therefore the linear wave theory cannot be applied to evaluate the wave energy flux in the surf zone. However, β is between 2 and 3.5, and then it can be said that $\beta\cong2.5$ is well approximated value. The value of γ changes according to breaker types and bottom slopes, and larger values of γ on steeper slope agree well with the foregoing studies.

3.4 Wave energy dissipation rate

Figure 16 shows variations of the nondimensional wave energy dissipation rate, Φ/Φ_{max} with X^*, where Φ_{max} is the maximum value of wave energy dissipation rate. The wave energy dissipation rate Φ is not constant, but it changes with X^*, depending on beraker types and the bottom slope.

In case of spilling breakers, Φ is small at the inception of wave breaking, but it gradually increases and becomes maximum around $X^*=0.8Xa$ ($X^*=0.45$ for case 1-1 and $X^*=0.8$ for case 2-1).

In the cases of plunging and heavy plunging breakers, different from spilling breakers, the wave energy dissipation rate Φ becomes larger at the inception of wave breaking, and takes a maximum value around $X^*=Xp$. The wave energy dissipation rate Φ becomes small in the range of $X^*>Xa$. As shown in Fig.16, rapid energy dissipation takes place in the order of spilling, plunging and heavy plunging breakers.

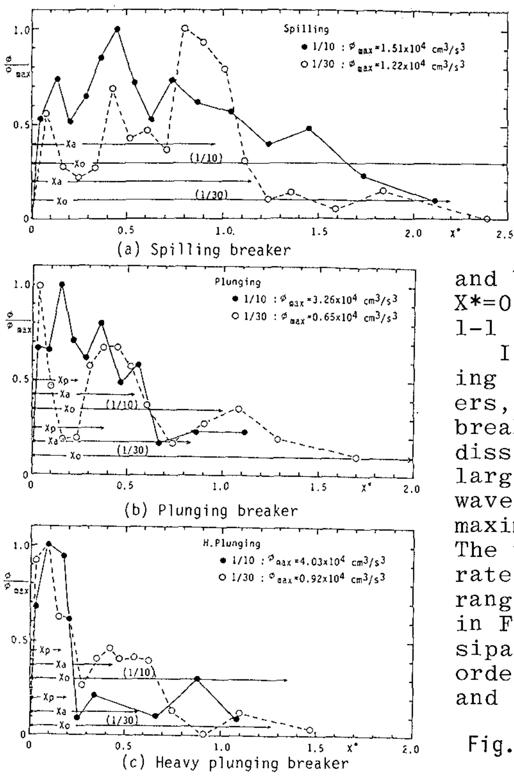

Fig.16 Variation of wave energy dissipation rate

3.5 Velocity of wave energy transport

Figure 17 shows two examples of variation of the non-dimensional velocity of wave energy transport Ce/Ceb with X*, in which Ceb is the value of Ce at X*=0, and Ce is defined with

$$Ce = F/E_T \qquad (11).$$

The group velocity Cg and the wave celerity C given by Airy wave theory are also drawn as solid and dotted lines, respectively, for comparison.

$$Cg = \frac{1}{2}\left(1+ \frac{2kh}{\sinh\, 2kh}\right)C \qquad (12) \qquad C = \frac{gL}{2\pi}\tanh\frac{2\pi h}{L} \qquad (13)$$

The velocity of wave energy transport Ce is , in general, in good agreement with the group velocity Cg before wave breaking takes palce, as shown in Fig.17. On the other hand, the velocity of energy transport Ce after breaking becomes smaller than the group velocity Cg and the difference between Ce and Cg becomes maximum around X*=0.8Xa∿Xa, in which the kinetic wave energy is much larger than the potential one, as already shown in Figs.10,11 and 12. This discrepancy of Ce from Cg is possibly caused by increasing of the offshore steady-velocity below the wave trough as in Fig.8.

The velocity of wave energy transport Ce is seen to close to the group velocity Cg in X*>Xo, especially in the case of spilling breaker. Since the kinetic energy is almost equal to the potehtial one in X*>Xo. It seems that wave energy is transported with the group velocity under the condition that the kinetic is almost equal to the potential one. The same facts are seen in other experimental cases such as case 1-1,1-2,1-3 and 2-2.

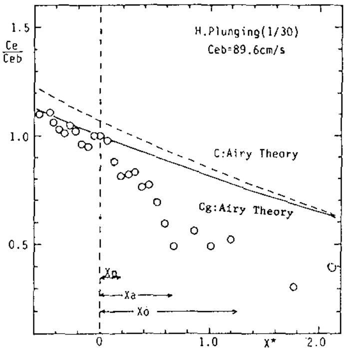

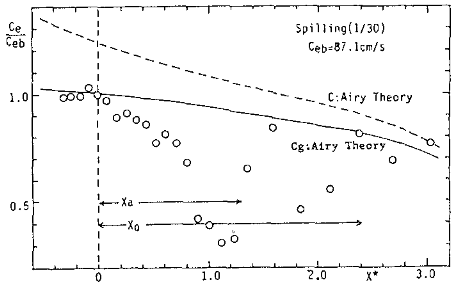

Fig.17 Relationship between Ce/Ceb and X*

4. CONCLUSION

The variation of the potential, kinetic and total wave energy after breaking has been discussed experimentally in relation to breaker types and bottom slopes. The main results obtained in this study are summarized as follows:

(1) The kinetic wave energy is larger than the potential

one in the surf zone. The ratio of the kinetic wave energy to the potential one is changed according to breaker types and bottom slopes. The location of the deepest air-entrained depth Xa, plunging point Xp, and location of air bubble's disappearance from wave body Xo can be indexes to the ratio of the kinetic wave energy to the potential one, from macroscopic viewpoint.

(2) Some of the potential wave energy can be transferred to the kinetic one at an early stage of wave breaking in the spilling breaker. The splash and the horizontal roller play an important role to the transfer mechanism between the kinetic and potential wave energy in plunging and heavy plunging breakers.

(3) The attenuation of the kinetic, potential and total wave energy becomes larger in the order of spilling, plunging, heavy plunging breakers. The magnitude of the attenuation increases with steepening of the bottom slope.

(4) The most of wave energy are dissipated in the region between the breaking point and the location of air bubble's disapperance from wave body (X*=Xo).

(5) The wave energy dissipation rate increases in the order of spilling, plunging and heavy plunging breakers. The location at which the maximum wave energy dissipation rate takes place approaches the breaking point in the order of spilling, plunging and heavy plunging breakers.

REFERENCES

Dean,R.G.(1965): Stream function representation of nonlinear ocean waves, Jour.of Geophy.Res.,Vol.70,pp.4561 - 4572.

Horikawa,K.and C.T.Kuo(1966): A study on wave transformation in the surf zone, Proc. 10th ICCE,pp.217 - 233.

Ishii,H.(1990): Variation of wave energy after breaking on slopes, Master thesis to Nagoya Univ.,21p.

Iwata,K.,Koyama,H.and S.Futo(1983): Experimental study on change of wave energy after breaking, Proc. 30th Japanese Conf. on Coastal Eng.,pp.10 - 14 (in Japanese).

Koyama,H. and K.Iwata(1986): Estimation of water particle velocities of shallow water waves by a modified transfer function method, Porc.20th ICCE,pp.425 - 436.

Lee,J.J.,Skjelbreia,J.E. and F.Raichlen(1982): Measurement of velocities in solitary waves,Jour.of waterway,port, coast and ocean Div.,Vol.108,No.WW2,ASCE,pp.200 - 218.

Nadaoka,K.,Kondoh,T. and N.Tanaka(1982): The structure of velocity field within the surf zone revealed by means of Laser-Doppler Anemometry, Rept.of the Port and Harbour Res.Inst.,Vol.21,pp.49 - 106.

Sawaragi,T. and K.Iwata(1974): On wave deformation after breaking, Proc.14th ICCE,pp.481 - 499.

Tsuchiya,Y.and S.Tsutsui(1982): Wave energy distribution and wave breaking process, Proc.29th Japanese Conf. on Coastal Eng.,pp.125 - 129 (in Japanese).